Quantitative nanoscale monitoring the effect of annealing process on the morphology and optical properties of poly(3-hexylthiophene)/[6,6]-phenyl C_{61}-butyric acid methyl ester thin film used in photovoltaic devices

Yu-Ching Huang,[1] Shang-Yu Chuang,[1] Ming-Chung Wu,[1] Hsuen-Li Chen,[1] Chun-Wei Chen,[1] and Wei-Fang Su[1,2,a)]
[1]*Department of Materials Science and Engineering, National Taiwan University, Taipei 106-17, Taiwan*
[2]*Institute of Polymer Science and Engineering, National Taiwan University, Taipei 106-17, Taiwan*

(Received 20 May 2009; accepted 29 June 2009; published online 13 August 2009)

We have studied the nanoscale changes in morphology and optical properties during annealing for bulk-heterojunction poly(3-hexylthiophene) (P3HT) and [6,6]-phenyl C_{61}-butyric acid methyl ester (PCBM) composite film. Thermal atomic force microscopy was used to monitor the morphology evolution of the film *in situ* quantitatively, which showed a migration and aggregation of PCBM with increasing temperature. Scanning near-field microscopy was used to investigate the quantitative changes in absorption behavior of the film in nanoscale with increasing annealing time at 140 °C, which indicated that the extent of absorption of the film was increased with increasing annealing time. However, a large PCBM aggregate (1 μm) was formed after the film annealed at 140 °C for 1 h. The aggregate interrupted the bicontinous morphology of the film and further affected the absorption behavior in nanoscale. Furthermore, the refractive index and extinction coefficient of the films increased after annealed 30 min at 140 °C, but decreased after an extended annealing for 60 min. The increase in optical properties indicated the film achieving a highly ordered structure upon heating. The results suggested that an optimized annealing process was at 140 °C for 30 min. Finally, devices with different annealing times at 140 °C were fabricated and evaluated. The highest charge mobility and power conversion efficiency of the device were fabricated as suggested annealing conditions. The nanoscale monitoring of the P3HT/PCBM film has been found to be very useful to determine the optimized annealing conditions for high efficiency photovoltaic device. © *2009 American Institute of Physics*. [DOI: 10.1063/1.3187930]

I. INTRODUCTION

Polymer solar cells have emerged as a promising cost-effective alternative to silicon-based solar cell. Some of the attractive advantages of polymer solar cells include ease of processing, mechanical flexibility, light weight, large area, and low cost.[1,2] The blend of regioregular poly(3-hexylthiophene) (P3HT) as the electron donor and [6,6]-phenyl-C_{61} butyric acid methyl ester (PCBM) as the electron acceptor is the most common active layer system studied for polymer solar cell, which has achieved a power conversion efficiency of 4%–5%.[3–7]

The performance of the polymer solar cell has been found to be dependent on the morphology of the active layer.[8–10] Many factors affect the morphology dramatically, such as the composition of the blend, the solvent used,[2,11] and the annealing process.[2,12–14] Thermal annealing, in particular, has been used extensively to improve the cell performance. In the P3HT/PCBM blend system, a bicontinous phase of crystallized P3HT and PCBM nanoaggregate is formed during the annealing process.[15–17] The effects of the annealing process on the morphology changes in the active layer have been studied for the annealed samples. The analysis of change in film morphology could improve the performance of devices due to the increasing crystallinity and PCBM aggregation.[18] Moreover, as thermal annealing temperatures approach the glass transition temperature, the formation of nanodomains within the matrix could modify charge transport pathways then enhance the performance.[19] Furthermore, atomic force microscopy (AFM) and UV-vis absorption spectrum have been used to explain the effect of thermal annealing temperature and time on the performance of devices.[20] However, monitoring the morphology evolution in nanoscale during anneal processing has never been done before. We have used AFM equipped with a heating apparatus (thermal AFM) to study the nanoscale morphology change *in situ* at nanoscale. The AFM tip can scan the specific area of the film upon heating. We can observe the changes in the surface at different temperatures in depth and clearly. Thermal AFM is a powerful tool to determine the optimum processing condition.

The changes in morphology also affect the absorption behaviors, correspondingly, the light harvest efficiency. The high absorption behaviors can result in a high short-circuit current.[21,22] Therefore, we investigate the annealing effect on the optical properties at nanoscale by means of scanning probe microscopy equipped with near-field spectroscopy (SNOM). The SNOM is a novel and powerful technique that allows two-dimensional mapping of current and absorption in fully fabricated organic solar cells.[23,24] The SNOM is also used to study the optical and electronic properties of conjugated polymer blends.[25,26] The SNOM is a scanning probe

a)Electronic mail: suwf@ntu.edu.tw.

technique in which a probe having a nanoscale aperture is held within the near field of a sample surface. This permits the optical properties of a surface to be resolved at a length scale significantly smaller than its diffraction limit.[27] We demonstrate the nanoscale changes in absorption behavior in active layer varied with different annealing times by using the SNOM. In addition, the optical constants of the composite film under different annealing conditions by ellipsometric measurements were carried out to model the light absorption behavior in organic photovoltaic devices.[28,29] We can calculate the refractive index (n) and the extinction coefficient (k) under different annealing conditions and then find the most appropriate process conditions to achieve the best performance.

Furthermore, we calculate the change in mobility under different annealing processes by means of space charge limited current (SCLC) model. Numerical modeling is used to understand the basic physics of device operation.[30,31] The SCLC is an ideal model to observe the blends of conjugated polymers and fullerenes since the system exhibits unbalanced charge transport, long exciton life-time, high charge carrier generation efficiency, and low mobility of the slowest charge carrier.[32] We use this method to understand the effect of annealing process on the changes in mobility.

II. EXPERIMENTAL DETAILS

The P3HT/PCBM film was made from a blend of P3HT and PCBM in 1:0.8 wt/wt ratio. P3HT (Mw =59 750 g mol^{-1}, PDI=1.5, regioregularity is about 96% as determined by NMR, synthesized in house) and PCBM (Aldrich Chemical) were dissolved in chlorobenzene and stirred for 1 h at 50 °C in the glovebox. The P3HT/PCBM film was spin coated at 700 rpm for 60 s on the indium-tin-oxide (ITO) glass. The ITO glass substrate covered with a 140 nm thick layer of indium tin oxide was first ultrasonically cleaned in a series of organic solvents (ethanol, methanol, and acetone).

The surface morphology evolution of the P3HT/PCBM film was measured by using AFM (Digital Instruments, Nanoscope III). We also used the AFM equipped with thermal apparatus (thermal AFM) to study the morphology evolution with temperature in air. Thermal AFM used an extra controller to apply heat to the sample and control the temperature of the sample, and the schematic is shown in Fig. 1. In thermal-AFM experiment, the instrument temperature was increased at 5 °C/min to a desired temperature and then held for 2 min to establish good temperature correlation between instrument and sample before AFM images are captured. The changes in morphology with gradually increasing temperature can be monitored, and the suitable temperature for the upcoming anneal process can be determined. Next, the AFM morphology studies were performed for film samples annealed at the specific temperature for different durations; this result will guide us a proper anneal condition to fabricate solar cells.

The nanoscale optical properties of the P3HT/PCBM film were studied in the transmission mode using the SNOM (WITec, AlphaSNOM, Germany) head with a special probe.

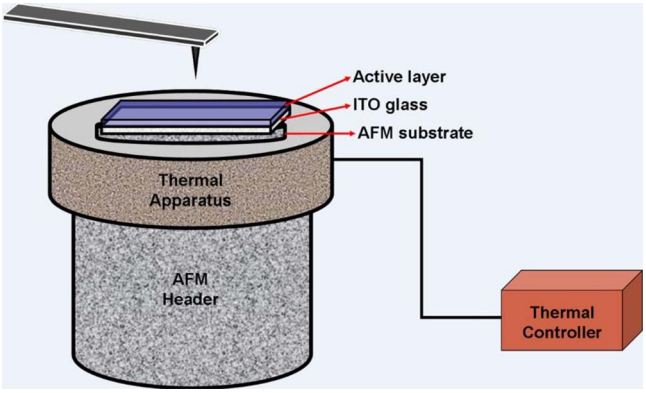

FIG. 1. (Color online) Schematic of thermal AFM experiment setup.

The special probe with microfabricated cantilever SNOM sensors (aperture ~100 nm) exhibited high transmission efficiency. An argon ion laser (488 nm) was employed as a radiation source. The transmitted light was collected by a 40× objective and detected by a single photon counting photomultiplier tube. For each line scan, 256 data points were taken with the line scan frequency to be 0.5 Hz. In all cases, the laser beam was focused down through a 100×, numerical aperture (NA) ~0.95 objective (Olympus, IX-70) on the inverted optical microscope.

For optical measurement, the P3HT/PCBM film was spin coated directly on the substrate, BK7, and the optical glass was cleaned in an ultrasonic bath using acetone and isopropanol then rinsed with de-ionized water and dried with nitrogen. The film thickness was determined by an α-stepper (Veeco, Dektak 6M 24383). The optical constants (n,k) of the organic layer were determined by an ellipsometer and calculated using a computer software. The ellipsometer consisted of a broadband photon source followed by a polarizer and a retarder. The polarized broadband light was incident to the sample and the reflected beam entered a monochromator after passing an analyzer. Light intensity was measured by a detector placed behind the monochromator. Ellipsometric parameters, tan Ψ and cos Δ data from 350 to 850 nm, were acquired in reflection mode at 75° of the incident angle. The transmittance and reflectance of the film were measured using an optical spectrometer (Hitachi, U-4100). The data were fitted to a mathematical dispersion function, also called oscillator model, describing dielectric function. Oscillator models required only a few oscillator coefficients to describe both the real and imaginary parts of the refractive index accurately over a very wide spectral range. Classical Lorentz oscillator's model was applied for this work.

The photovoltaic devices were fabricated by spin coating the P3HT/PCBM blend on the ITO glass, which was covered with a 40 nm thick layer of poly (3,4-ethylenedioxythiophene)-poly(styrenesulfonate) (PEDOT:PSS) (Baytron P, 4083). After coating with PEDOT:PSS and baking at 120 °C for 30 min in the oven, the substrates were transferred to a nitrogen filled glovebox (<0.1 ppm for O_2 and H_2O). The cathode of Al (~120 nm) was deposited on the top of the P3HT/PCBM layer by thermal deposition after different annealing conditions. The performance of these de-

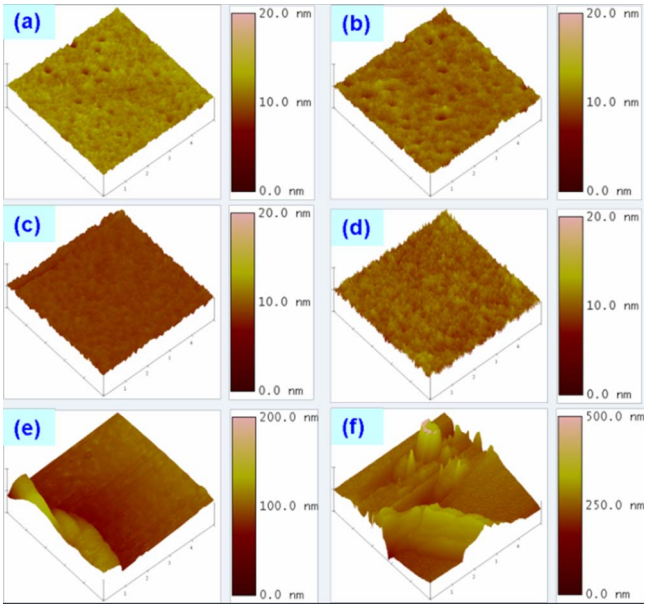

FIG. 2. (Color online) Thermal AFM images of the P3HT/PCBM film under different temperatures: (a) 25, (b) 90, (c) 110, (d) 130, (e) 140, and (f) 150 °C.

vices was evaluated under AM 1.5G irradiation (100 mW cm^{-2}) using a solar simulator (Oriel Inc.).

III. RESULTS AND DISCUSSION

We fabricate the P3HT/PCBM composite film on an ITO substrate and then, by using thermal AFM, monitor surface morphology changes *in situ* with changing temperature; these images are shown in Fig. 2. The morphology of the P3HT/PCBM composite thin film changes slightly when the temperature is increased gradually (5 °C/min) from room temperature to 130 °C. At 130 °C, some needlelike aggregations arise on the surface of the film. Large aggregation appears as the temperature reaches 140 °C, and its amount increases dramatically at 150 °C due to the soft P3HT chain that allows the PCBM particles to move easily. The aggregate is confirmed to be PCBM molecules from our previous study.[17] The PCBM is dispersed evenly in the P3HT matrix initially but it undergoes phase separation and aggregation after heat treatment. The extent of morphology change can be quantitatively determined using surface roughness (rms) value as shown in Fig. 3. We observe that the rms roughness first increases slightly (0.72–1.66 nm) from 25 to 110 °C then decreases (1.37 nm) at 120 °C, which is the glass transition temperature (Tg) of P3HT. At its Tg, P3HT chains are soft and flexible and the surface of the composite film becomes flatter than that at lower temperature (1.37 nm versus 1.66 nm). At 140 °C (above Tg), the PCBM particles are aggregated easily inside soft P3HT that results in a large extent of phase separation. Thus, the roughness of the P3HT/PCBM film increases extensively. In this investigation, we have comprehended the nanoscale surface morphology variation of the P3HT/PCBM film quantitatively at different temperatures using thermal AFM. The results indicate that the temperature of 140 °C is suitable for a P3HT/PCBM film to obtain the desired phase separation for solar cell application.

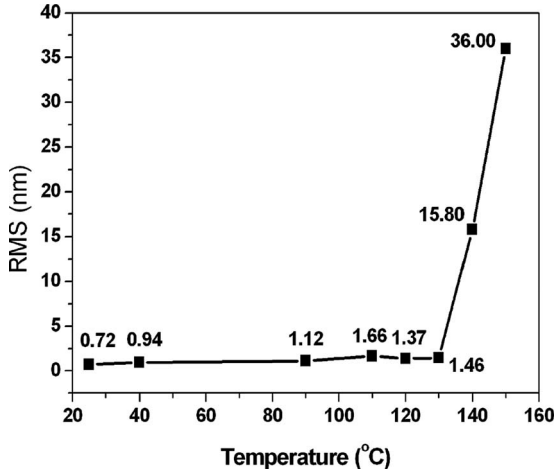

FIG. 3. The change in rms value of the P3HT/PCBM film under different temperatures.

Therefore, 140 °C is set for the annealing temperature in the following study of anneal time effect on the morphology evolution of the P3HT/PCBM composite film.

Four samples were annealed at 140 °C for 0, 10, 30, and 60 min, respectively, and then they were evaluated by room temperature AFM. The thermal AFM was not used here because the thermal fluctuation of the AFM tip is too large to have accurate surface profile measurement with scanning time longer than 10 min at 140 °C. The surface of the film without annealing is very smooth with a rms roughness of 1.53 nm [Fig. 4(a)]. The roughness increases gradually to 1.86 nm for 10 min annealing [Fig. 4(b)], further to 2.46 nm for 30 min annealing [Fig. 4(c)], then to a very large roughness of 19.08 nm due to the formation of large aggregates after 60 min annealing [Fig. 4(d)]. The surface roughness of the thermal AFM studied sample at 140 °C is higher than that of the annealed sample of 140 °C for 30 min (15.8 nm versus 2.46 nm), which is due to the cumulated thermal history of the former (about 40 min heating above Tg). Nevertheless, the results of the AFM studies of annealed samples at room temperature imply that the annealing condition of 140 °C for 30 min is a good processing condition to obtain desired phase separation without large aggregation. The bicontinuous phase formation in the P3HT/PCBM film facili-

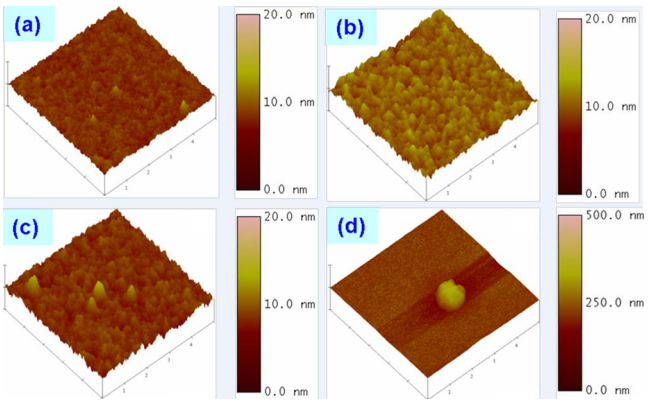

FIG. 4. (Color online) 3D topography images of the P3HT/PCBM film after different annealing times at 140 °C: (a) without annealing, (b) 10 min, (c) 30 min, and (d) 60 min.

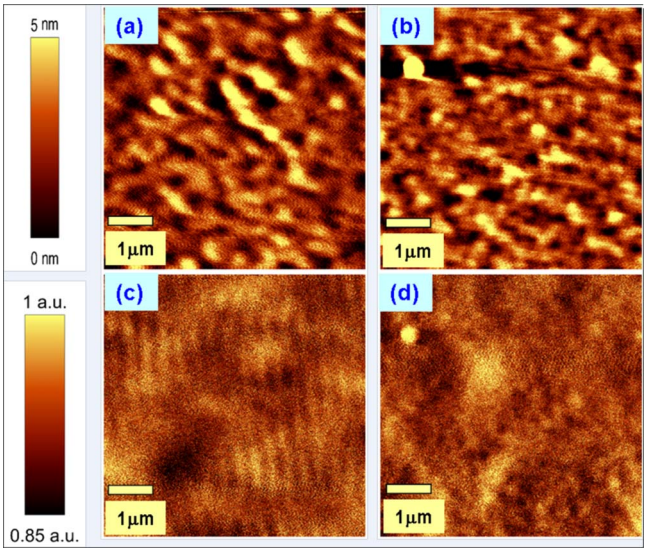

FIG. 5. (Color online) SNOM images under transmission mode using monochromatic laser radiation at 488 nm for P3HT films. (a) and (c) are topographic and SNOM images, respectively, for sample without annealing. (b) and (d) are topographic and SNOM images, respectively, for sample annealed at 140 °C for 30 min.

tates efficient charge separation and transport, increases current density, and enhances the internal light scattering and absorption that will be discussed later in detail.

The SNOM can simultaneously monitor the morphology and absorption behavior of a thin film. Therefore, we use it to map the absorption distribution and quantify the absorbance. A SNOM probe with an aperture of around 100 nm in diameter on the sharp end is placed in the near field of the investigated sample. High-quality optical contrast images can be obtained by this technique. We first investigate the effect of the anneal process on pristine P3HT films since the main absorption peak comes from the P3HT. The surface topography and absorption contrast images of the two pristine P3HT thin films with different annealing processes are shown in Fig. 5. Both pristine P3HT films exhibit smooth surface topography whether the film is unannealed [Fig. 5(a)] or annealed [Fig. 5(b)]. The pristine P3HT film without annealing shows a homogeneous absorption behavior [Fig. 5(c)], which is due to the uniform distribution of the P3HT thin film. After annealing at 140 °C for 30 min, the surface morphology does not change much but the absorption behavior shows some variations [Fig. 5(d)]. The contrast of the absorption image of an annealed sample is higher than that of an unannealed sample. The increased contrast is due to improved interchain stacking, conjugation, and delocalization of P3HT. Then, we studied the absorption behavior of the P3HT/PCBM film using SNOM. As shown in Figs. 6(a)–6(d), we could observe that the size of the PCBM aggregate becomes larger with increasing annealing time; the results are in agreement with the AFM studies (Fig. 4). Figure 6(e) shows the homogenous absorption distribution for the composite film without annealing. As the annealing time increases and the surface morphology changes, the contrast of the absorption becomes high and the distribution is very inhomogeneous [Figs. 6(f)–6(h)]. The high contrast of the absorption is due to the good interchain stacking of P3HT

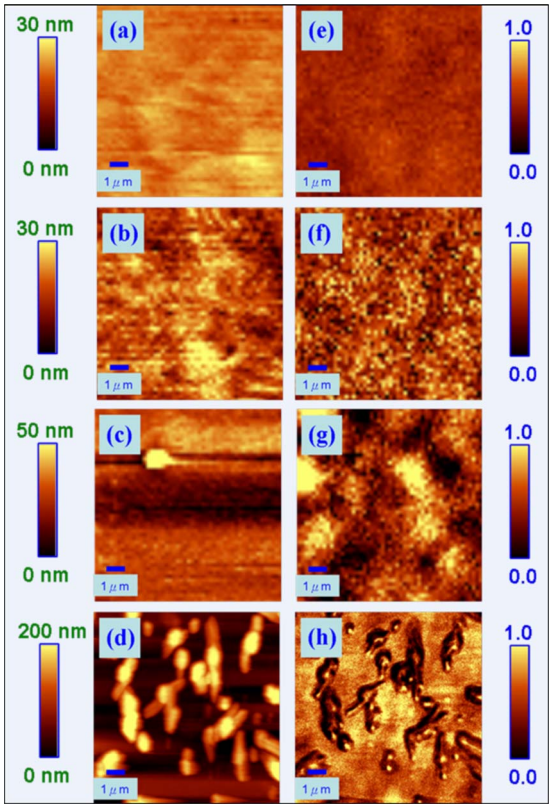

FIG. 6. (Color online) SNOM images under transmission mode using monochromatic laser radiation at 488 nm for P3HT/PCBM thin films. (a)–(d) are topographic images and (e)–(h) are SNOM images. The samples are annealed at 140 °C for 0, 10, 30, and 60 min, respectively.

crystallization accompanied with the annealing process, and the inhomogeneous absorption distribution is from the phase separation and formation of PCBM aggregation. The P3HT-rich region reveals stronger absorbance than that of the PCBM-rich region. The phase separation of the blend is known to improve the charge separation and transport at the boundary of donor and acceptor and further improves the power conversion efficient.[15,17] Here, we also present that crystallization and adequate phase separation can improve the extent of light absorption with increased exciton generation. However, when the sample is annealed at 140 °C for 60 min, large PCBM aggregations can block the light and decrease the absorption in average [Fig. 6(d)]. Thus, the nanoscale absorption images probed by SNOM provide direct information about the interplay between topography and the absorption density of the P3HT/PCBM film. Both AFM and SNOM technique determine that an optimized annealing process at 140 °C for 30 min will provide the P3HT/PCBM film with improved crystallinity and with adequate phase separation for an efficient solar cell.

We further investigate the relationship between the annealing process and the optical properties of the P3HT/PCBM film using ellipsometric and optical measurements. The optical constants (n,k) of the films with different annealing times at 140 °C are determined at a wavelength, which ranged from 350 to 800 nm. The peaks of the optical curves are redshifted due to the enhanced intermolecular order from flatter molecular conformation and reduced torsion of P3HT

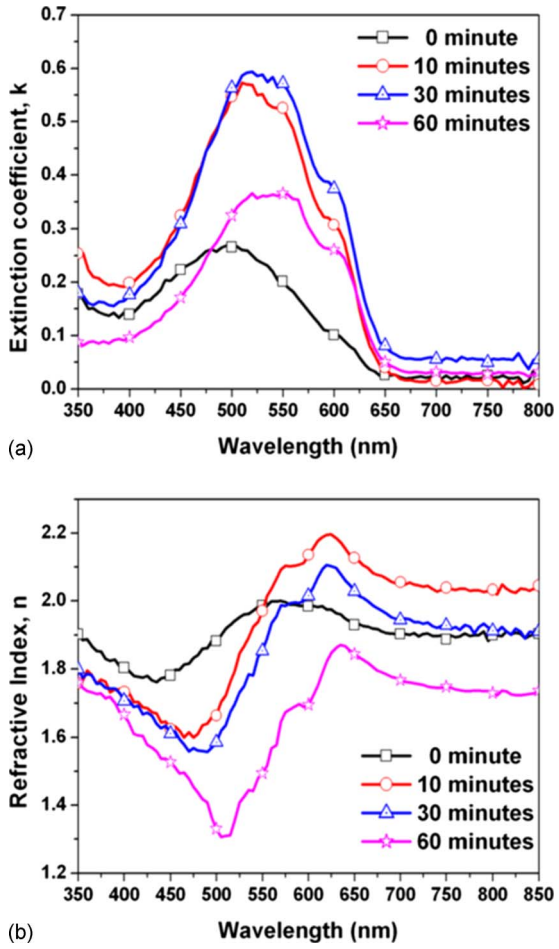

FIG. 7. (Color online) Optical constants' measurements of the P3HT/PCBM films annealed at 140 °C for different durations. (a) Extinction coefficient (k) and (b) refractive index (n).

after annealing (Fig. 7). Up to 30 min annealing, Fig. 7(a) shows that the major absorption peak of π-π^* of the film has increased intensity and been redshifted from 500 to 520 nm after annealing due to increased crystallization from π-π stacking of P3HT. The intensities of the two vibronic peaks of 550 and 600 nm of annealed samples are also increased. Thus, the extinction coefficient of the film increased from 0.27 to 0.59. However, the value is decreased to 0.36 after the film annealed for 60 min, which is due to the large PCBM aggregate formation with lowered P3HT crystallization. Figure 7(b) shows that the refractive index abnormal dispersion curves are peaked at 2.2 and 2.11 for 10 and 30 min annealed samples, respectively, as compared with 1.95 of unannealed sample. The increased refractive index of annealed samples is due to the increased density from P3HT crystallization. However, the crystallization is disrupted with excessive annealing for 60 min, which results in a lower refractive index of 1.87.

Next, we fabricate P3HT/PCBM bulk-heterojunction photovoltaic devices under different annealing durations at 140 °C. Figure 8 shows the mobility of the P3HT/PCBM film measured by SCLC. The thickness of the films is all kept around 100 nm. The mobility of the device is increased with increasing annealing time but is decreased for 60 min duration. The high mobility indicates an improved charge

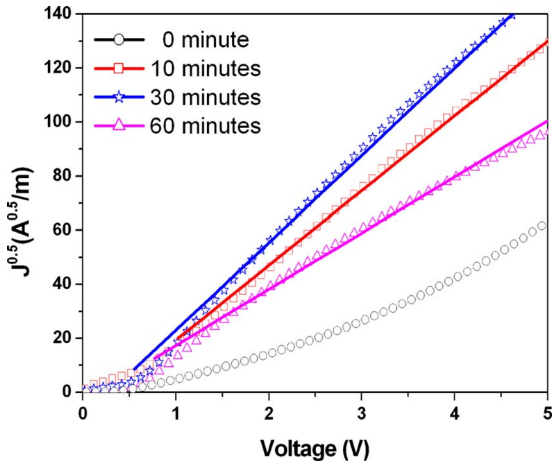

FIG. 8. (Color online) Mobility characteristics of photovoltaic devices based on the P3HT/PCBM films annealed at 140 °C for different times under A.M. 1.5 illumination (100 mW/cm^2).

separation and transport due to the phase separation between P3HT and PCBM. A large extent of phase separation reduces the bicontinuous phases present in the composite thin film, thus decreases its mobility. Figure 9 shows the I-V curves of the solar cell measured under A.M. 1.5 illumination. The performance of the solar cell is also improved with increasing annealing time up to 30 min. The slight increase in open-circuit voltage (V_{oc}) is attributed to the reduction in back charge recombination rate at the P3HT/PCBM interfaces with increased order structure upon annealing. The short-circuit current density (J_{sc}) has increased by about 75% due to the improved absorption behavior and the enhanced charge mobility. We can observe a large improvement in fill factor after the annealing process, and this may be due to the reduced serial resistance and increased carrier mobility as a result of highly order polymer chains. However, the annealing process at 140 °C for 60 min decreases the solar cell performance. The formation of large PCBM aggregation interrupts the charge transport and increases the chance of short circuit, resulting in poor device performance. The best performance of the solar cell is achieved when the cell is

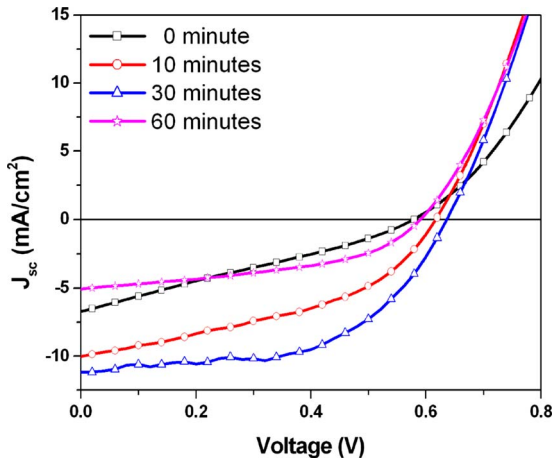

FIG. 9. (Color online) IV characteristics of photovoltaic devices based on the P3HT/PCBM films annealed at 140 °C for different times under A.M. 1.5 illumination (100 mW/cm^2).

TABLE I. Mobility and performance of the P3HT/PCBM solar cells under A.M. 1.5 illumination (100 mW/cm^2) annealed at 140 °C for different times.

Annealing time (min)	V_{oc} (V)	J_{sc} (mA/cm^2)	FF (%)	η (%)	Mobility (cm^2/V s)
0	0.58	6.72	27.14	1.06	2.51×10^{-05}
10	0.62	10.02	42.32	2.61	2.01×10^{-03}
30	0.64	11.15	54.27	3.85	2.64×10^{-03}
60	0.59	5.06	44.90	1.35	1.02×10^{-03}

annealed at 140 °C for 30 min and an efficiency of 3.85% under A.M. 1.5 illumination is found. The mobility and performance solar cells with different annealing treatments are summarized in Table I.

IV. CONCLUSION

We have investigated the effect of annealing process on the performance of photovoltaic devices based on P3HT/PCBM blend materials by monitoring the changes in nanoscale morphology and optical properties. The thermal AFM provides valuable information of morphology evolution quantitatively for the P3HT/PCBM film during the annealing process. The SNOM and optical constants' measurements provide additional information in the changes in nanoscale absorption behavior upon heating. The results help to determine an optimized annealing process for high performance solar cell. Thus, the device performance improves from 1.06% to 3.85% after annealing at 140 °C for 30 min, then decreases to 1.35% with 60 min annealing.

ACKNOWLEDGMENTS

The financial support from the National Science Council of Taiwan (Grant Nos. NSC-96-2628-E-002-017-MY3 and NSC 95-3114-P-002-003-MY3) is highly appreciated. The authors would also like to thank Mr. Y. Y. Lin and Miss Sharon Chen of the National Taiwan University for helpful discussions.

[1]W. Ma, C. Yang, X. Gong, K. Lee, and A. J. Heeger, Adv. Funct. Mater. **15**, 1617 (2005).
[2]G. Li, V. Shrotriya, J. Huang, Y. Yao, T. Moriarty, K. Emery, and Y. Yang, Nature Mater. **4**, 864 (2005).
[3]G. Yu, J. Gao, J. C. Hummelen, F. Wudl, and A. J. Heeger, Science **270**, 1789 (1995).
[4]M. Granström, K. Petritsch, A. C. Arias, A. Lux, M. R. Andersson, and R. H. Friend, Nature (London) **395**, 257 (1998).
[5]C. J. Brabec, N. S. Sariciftci, and J. C. Hummelen, Adv. Funct. Mater. **11**, 15 (2001).
[6]Y. Kim, S. Cook, S. M. Tuladhar, S. A. Choulis, J. Nelson, J. R. Durrant, D. D. C. Bradley, M. Giles, I. Mcculloch, C.-S. Ha, and M. Ree, Nature Mater. **5**, 197 (2006).
[7]C. Zhang, S. W. Tong, C. Jiang, E. T. Kang, D. S. H. Chan, and C. Zhu, Appl. Phys. Lett. **93**, 043307 (2008).
[8]H. Hoppe and N. S. Sariciftci, J. Mater. Res. **19**, 1924 (2004).
[9]H. Hoppe and N. S. Sariciftci, J. Mater. Chem. **16**, 45 (2006).
[10]M. Campoy-Quiles, T. Ferenczi, T. Agostinelli, P. G. Etchegoin, Y. Y. Kim, T. D. Anthopoulos, P. N. Stavrinou, D. D. C. Bradley, and J. Nelson Nature Mater. **7**, 158 (2008).
[11]M. Al-lbrahim, O. Ambacher, S. Sensfuss and G. Gobsch, Appl. Phys. Lett. **86**, 201120 (2005).
[12]F. Padinger, R. S. Rittberger, and N. S. Sariciftci, Adv. Funct. Mater. **13**, 85 (2003).
[13]X. N. Yang, J. K. J. Van Duren, M. T. Rispens, J. C. Hummelen, R. A. J. Janssen, M. A. J. Michels, and J. Loos, Adv. Mater. (Weinheim, Ger.) **16**, 802 (2004).
[14]L. H. Nguyen, H. Hoppe, T. Erb, S. Günes, G. Gobsch, and N. S. Sariciftci, Adv. Funct. Mater. **17**, 1071 (2007).
[15]X. Yang, J. Loos, S. C. Veenstra, W. J. H. Verhees, M. M. Wienk, J. M. Kroon, M. A. J. Michels, and R. A. Janssen, Nano Lett. **5**, 579 (2005).
[16]X. N. Yang, A. Alexeev, M. A. J. Michels, and J. Loos, Macromolecules **38**, 4289 (2005).
[17]Y. C. Huang, Y. C. Liao, S. S. Li, M. C. Wu, C. W. Chen, and W. F. Su, Sol. Energy Mater. Sol. Cells **93**, 888 (2009).
[18]M. Reyes-Reyes, K. Kim, and D. L. Carroll, Appl. Phys. Lett. **87**, 083506 (2005).
[19]K. Kim, J. Liu, M. A. G. Namboothiry, and D. L. Carroll, Appl. Phys. Lett. **90**, 163511 (2007).
[20]G. Li, V. Shrotriya, Y. Yao, and Y. Yang, J. Appl. Phys. **98**, 043704 (2005).
[21]V. Shrotriya, E. H. Wu, G. Li, Y. Yao, and Y. Yang, Appl. Phys. Lett. **88**, 064104 (2006).
[22]A. K. Pandey, S. D. Seignon, and J. M. Nunzi, Appl. Phys. Lett. **89**, 113506 (2006).
[23]C. R. Mcneill, H. Frohne, J. L. Holdsworth, and P. C. Dastoor, Nano Lett. **4**, 2503 (2004).
[24]E. Klimov, W. Li, X. Yang, G. G. Hoffmann, and J. Loos, Macromolecules **39**, 4493 (2006).
[25]P. F. Barbara, D. M. Adams, and D. B. O'Conner, Annu. Rev. Mater. Sci. **29**, 433 (1999).
[26]A. Cadby, R. Dean, A. M. Fox, R. A. L. Jones, and D. G. Lidzey, Nano Lett. **5**, 2232 (2005).
[27]E. Hecht, *Optics*, 3rd ed. (Addison-Wesley, Reading, MA, 1998).
[28]D. P. Gruber, G. Meinhardt, and W. Papousek, Sol. Energy Mater. Sol. Cells **87**, 215 (2005).
[29]A. J. Moule and K. Meerholz, Appl. Phys. B: Lasers Opt. **86**, 721 (2007).
[30]P. W. M. Blom, V. D. Mihailetchi, L. J. A. Koster, and D. E. Markov, Adv. Mater. (Weinheim, Ger.) **19**, 1551 (2007).
[31]E. C. P. Smits, S. G. J. Mathijssen, M. Colle, A. J. G. Mank, P. A. Bobbert, P. W. M. Blom, B. de Boer, and D. M. de Leeuw, Phys. Rev. B **76**, 125202 (2007).
[32]V. D. Mihailetchi, J. Wildeman, and P. W. M. Bolm, Phys. Rev. Lett. **94**, 126602 (2005).